Experimental Demonstration of Mid-Infrared Holey and Slotted Photonic Crystal Waveguides in Silicon on Sapphire

Yi Zou,[1] Parker Wray,[1] Swapnajit Chakravarty,[2] and Ray T. Chen[1,2]
[1]*Microelectronics Research Center, Electrical and Computer Engineering Department, University of Texas at Austin, Austin, TX, 78758, USA*
[2]*Omega Optics Inc., Austin, TX, 78759, USA*
Author e-mail address: yzou@utexas.edu, swapnajit.chakravarty@omegaoptics.com, raychen@uts.cc.utexas.edu

Abstract: We provide the first experimental demonstration of propagation characteristics of holey and slotted two dimensional photonic crystal waveguides in silicon-on-sapphire at mid-infrared wavelength of 3.43μm.

OCIS codes: (230.5298) Photonic crystals; (130.5296) Photonic crystal waveguides; (130.3120) Integrated Optics Devices;

Silicon has been the material of choice of the photonics industry over the last decade due to its easy integration with silicon electronics as well as its optical transparency in the near-infrared telecom wavelengths. Slow light in photonic crystal waveguides (PCWs) [1] and slotted PC waveguides (SPCW) [2], [3] has been used to reduce the optical absorption path length and achieve high detection sensitivity in on-chip optical absorption spectroscopy for the selective detection of volatile organic compounds (VOCs) [1], [2] and greenhouse gases [3] based on unique analyte absorption signatures in the near-infrared (near-IR). In the mid-infrared (mid-IR), most compounds and gases of interest, such as xylene and methane respectively, have at least two orders of magnitude larger absorption cross-sections than in the near-IR. Silicon-on-sapphire (SoS) (till 5.5μm) can serve as an ideal platform for highly sensitive optical absorption spectroscopy on chip in the mid-IR. PC research in the mid-IR has been limited by the need for bulky and expensive tunable laser sources [4], [5] and thus cannot be transitioned easily from the lab to the field.

Recently, we presented the first demonstration of photonic crystal waveguide (PCW) characteristics in SoS at the mid-IR wavelength 3.43μm with a fixed wavelength interband cascade laser (ICL) [6]. While slowdown of light increases the interaction time between the analyte and the propagating optical mode, in PCWs the optical interaction in the slow light regime is limited primarily to the in-plane evanescent optical mode overlap within the holes of the PC lattice, in the first two or three rows adjacent to the PCW. We previously demonstrated the enhanced detection sensitivity of VOCs in PC waveguides versus ridge and slot waveguides [7], [8], by infrared absorption spectroscopy on chip. SPCW devices provide enhanced optical absorbance by the analyte due to the combined effects of enhanced optical mode overlap with the analyte and large slow-down of light in the PCW. However, in the mid-IR, SPCW structures have not been experimentally demonstrated.

In this paper, we *experimentally investigate for the first time in the mid-IR, two structures that enable enhanced intensity overlap with the analyte within a slow light PCW. The first structure is a holey PCW (HPCW) wherein smaller diameter holes than* the bulk PC are etched along the propagation direction within the PCW at the antinodes of the PCW propagating mode. The second structure is a SPCW wherein a rectangular slot is etched uniformly at the center of the PCW from the input to the output.

Scanning electron micrograph (SEM) images of the HPCW and SPCW are shown in Figs. 1(a) and (d). The devices were fabricated in SoS with h=585 +/-1nm from ellipsometry for the HPCW and h=575 +/-1nm from ellipsometry for the SPCW. The fabrication details are described in our previous paper [9]. Figs. 1(b) and (e) show the dispersion diagram of the W1.2 HPCW and W1.5 SPCW obtained by 3D plane-wave expansion simulation respectively. Here W1.2 and W1.5 indicate that the width of the PCW at the onset of the taper is $1.2\times\sqrt{3}\ a$ and $1.5\times\sqrt{3}a$ respectively. For HPCW, at the center, a row of smaller holes with radius rs=0.625r, where r=0.25a is the radius of the holes in the bulk lattice, is etched at the lattice positions of the PC. For SPCW, the radius of air holes is r=0.25a. At the center of it, a rectangular slot with width s=0.155a, is etched from the input to the output. The dispersion diagram shows the guided mode separated from the dielectric band by a stop gap. The light line for sapphire is superimposed. The electric field intensity profile of the propagating slow light modes, indicated by the red circle in Figs. 1(b) and (e) are shown in Fig. 1(c) and (f). The light from the output SWG for short 50μm (~60 periods) long HPCW devices with several lattice constants but the same r/a is plotted in Fig. 2(a). The plot is normalized with respect to the highest and lowest power observed versus lattice constant. It is observed that for a less than 830nm, the output power from the devices is practically zero. Propagation loss measurements were done for several devices in Fig. 2(a) and plotted. Devices with lengths 50μm, 100μm, 200μm and 400μm were fabricated at a=840nm, 845nm, 850nm, 865nm, 870nm and 890nm. Transmission losses as observed in Fig. 2(c) were obtained. The measured propagation losses at a=840nm and 845nm are 15dB/cm and 13dB/cm respectively. At

a=850nm, 865nm, 870nm, and 890nm, the propagation loss increases rapidly with increasing lattice constant of the PCW, reaching as high as 900dB/cm for *a*=890nm. It can thus be concluded that the ICL emission propagates above the light line for devices with a greater than 845nm. When the device is immersed in tetrachloroethylene (C2Cl4), non-absorbing liquid at 3.43μm, the guided mode moves to lower frequency. Hence the fixed wavelength ICL can transmit light in devices with smaller lattice constant, as shown by the dashed curve in the inset of Fig. 2(a). Similar performances were observed on SPCW as shown in Figs. 2(b) and (d).

In summary, we demonstrated the propagation characteristics of holey and slotted PCWs in SoS at the mid-IR. By engineering the lattice constant, we experimentally demonstrated the transmission characteristics with a single wavelength source. In the guided mode region below the light line, propagation losses below 20dB/cm were observed for group indices n_g greater than 20 for the HPCW. Huge losses above the light line and zero transmission in the stop band were experimentally observed. Similar losses above the light line and in the stop gap were observed in SPCWs. Below the light line, propagation losses observed were similar to losses observed in similar devices in SOI in the near-infrared.

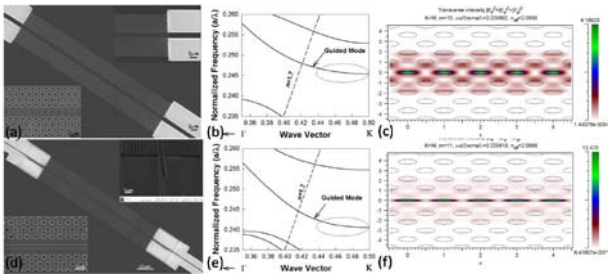

Fig. 1. HPCW (a)SEM images of fabricated devices on SoS substrate, (b) Dispersion diagram of the device in (a) by plane-wave expansion. (c) Electric field intensity profile of the propagating slow light mode at the Brillouin zone boundary. SPCW (d)SEM images of fabricated devices on SoS substrate, (e) Dispersion diagram of the device in (d) by plane-wave expansion. (f) Electric field intensity profile of the propagating slow light mode at the Brillouin zone boundary.

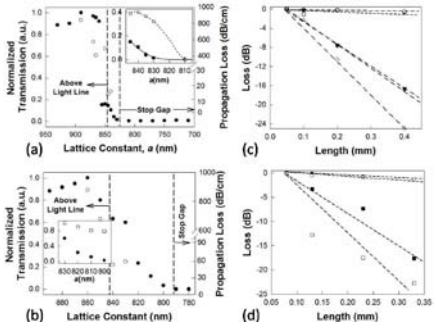

Fig. 2. HPCW (a) Normalized transmitted intensity through an air-clad W1.2 HPCW in SoS with r=0.25a, rs=0.625r as a function of a at λ=3.43μm plotted in air (bold circles). Propagation losses were measured for few devices (open circles). Insets magnify the data for devices between a=810nm and a=845nm in air (●) and tetrachloroethylene (□). (b) Propagation loss for devices of different length at a=840nm (●), a=845nm (○), a=850nm (□), a=865nm (■) and a=870nm (▲). SPCW (c) Normalized transmitted intensity through an air-clad W1.5 SPCW in SoS with r=0.25a, s=0.155a as a function of a at λ=3.43μm plotted in air (bold circles). Propagation losses were measured for few devices (open circles). Insets magnify the data for devices between a=830nm and a=800nm in air (●) and tetrachloroethylene (□). (d) Propagation loss for devices of different length at a=830nm (●), a=840nm (○), a=850nm (■) and a=860nm (□).

References

[1] W.-C. Lai, S. Chakravarty, Y. Zou, and R. T. Chen, "Multiplexed detection of xylene and trichloroethylene in water by photonic crystal absorption spectroscopy," Opt Lett **38**, 3799-3802 (2013).

[2] W.-C. Lai, S. Chakravarty, X. Wang, C. Lin, and R. T. Chen, "Photonic crystal slot waveguide absorption spectrometer for on-chip near-infrared spectroscopy of xylene in water," Applied Physics Letters **98**, 023304 (2011).

[3] W.-C. Lai, S. Chakravarty, X. Wang, C. Lin, and R. T. Chen, "On-chip methane sensing by near-IR absorption signatures in a photonic crystal slot waveguide," Opt Lett **36**, 984-986 (2011).

[4] C. Reimer, M. Nedeljkovic, D. J. Stothard, M. O. Esnault, C. Reardon, L. O'Faolain, M. Dunn, G. Z. Mashanovich, and T. F. Krauss, "Mid-infrared photonic crystal waveguides in silicon," Opt Express **20**, 29361-29368 (2012).

[5] R. Shankar, R. Leijssen, I. Bulu, and M. Lončar, "Mid-infrared photonic crystal cavities in silicon," Opt Express **19**, 5579-5586 (2011).

[6] Y. Zou, S. Chakravarty, P. Wray, and R. T. Chen, "Experimental Demonstration of Propagation Characteristics of Mid-Infrared Photonic Crystal Waveguides in Silicon-on-Sapphire," (Submitted).

[7] W.-C. Lai, Y. Zou, S. Chakravarty, L. Zhu, and R. T. Chen, "Comparative sensitivity analysis of integrated optical waveguides for near-infrared volatile organic compounds with 1ppb detection," in *SPIE OPTO*, (International Society for Optics and Photonics, 2014), 89900Z-89900Z-89906.

[8] Y. Zou, S. Chakravarty, W.-C. Lai, and R. Chen, "Silicon Chip Based Near-Infrared and Mid-Infrared Optical Spectroscopy for Volatile Organic Compound Sensing," in *CLEO: Science and Innovations*, (Optical Society of America, 2014), STh3M. 6.

[9] Y. Zou, H. Subbaraman, S. Chakravarty, X. Xu, A. Hosseini, W.-C. Lai, P. Wray, and R. T. Chen, "Grating-coupled silicon-on-sapphire integrated slot waveguides operating at mid-infrared wavelengths," Opt Lett **39**, 3070-3073 (2014).

Acknowledgements

The authors thank NSF for partially supporting this work (SBIR Grant #IIP-1127251). S.C., P.W and R.C acknowledge the Army SBIR Contract #W911SR-12-C-0046 for partially supporting this work.